Lead, zinc, and copper redistributions in soils along a deposition gradient from emissions of a Pb-Ag smelter decommissioned 100 years ago

Romain Gelly, Zuzana Fekiacova, Abel Guihou, Emmanuel Doelsch, Pierre Deschamps, Catherine Keller

▶ To cite this version:

HAL Id: hal-02073144
https://hal.science/hal-02073144

Submitted on 19 Mar 2019

Lead, zinc and copper redistributions in soils along a deposition gradient from emissions of a Pb-Ag smelter decommissioned 100 years ago

R. Gelly [1]*, *Z. Fekiacova* [1], *A. Guihou* [1], *E. Doelsch* [2], *P. Deschamps* [1], *C. Keller* [1]

(1) Aix Marseille Univ, CNRS, IRD, INRA, Coll France, CEREGE, BP 80, 13545 Aix-en-Provence cedex 04, France

(2) CIRAD, UPR Recyclage et risque, F-34398 Montpellier, France Recyclage et Risque, Univ Montpellier, CIRAD, Montpellier, France

17 <u>Abstract</u>

18 Sourcing and understanding the fate of anthropogenic metals in a historical contamination context

19 is challenging. Here we combined elemental and isotopic (Pb, Zn, Cu) analyses with X-ray

20 absorption spectroscopy (XAS) measurements (Zn) to trace the fate, in undisturbed soil profiles,

21 of historical metal contamination emitted by a 167-year-old Pb-Ag smelter decommissioned 100

22 years ago located in the Calanques National Park (Marseilles, France). Lead isotopic

23 measurements show that entire soil profiles were affected by 74 years of Pb emissions up to ~7

24 km from the smelter under the main NNW wind, and indicate particulate transfer down to 0.8 m

25 at depth. This vertical mobility of anthropogenic Pb contrasts with previous studies where Pb was

26 immobilized in surface horizons. The contribution of anthropogenic Pb to the total Pb

27 concentration in soils was estimated at 95% in surface horizons, and 78% in the deepest horizons.

28 Zinc isotopic signatures of past emissions, that are enriched in light isotopes compared to the

29 natural geological background (-0.69 ±0.03‰ and -0.15 ±0.02‰, respectively), were detected only

30 in the surface horizons of the studied soils. Using XAS analyses, we showed that anthropogenic

31 Zn was transformed and immobilized in surface horizons as Zn-Layered Double Hydroxide, thus

32 favoring the enrichment in heavy isotopes in these surface horizons. No clear evidence of copper

33 contamination by the smelter was found and Cu isotopes point to a bedrock origin and a natural

34 distribution of Cu concentrations.

35

36 <u>Highlights:</u>

37 • δPb, Zn, Cu in soils impacted by emissions 100 y ago from a smelter

38 • Pb contamination was detected 7 km away from the smelter and down the soil profiles

39   •   Light δ^{66}Zn values were measured in the chimney and in soil surface horizons

40   •   Precipitation of Zn-Layered Double Hydroxide prevented downwards migration of

41   anthropogenic Zn

42   •   Cu isotopes indicate its geogenic origin and redistribution in soils by pedogenesis

43

44   <u>Keywords</u>:

45   metal contamination, soil, stable isotopes, historical contamination, metal cycling, smelting

46

47   **Introduction**

48   Lead (Pb), zinc (Zn) and copper (Cu) are trace elements naturally present in soils at

49   concentrations usually below 1000 mg kg^{-1} (Kabata-Pendias, 2011). They are also released by

50   human activities through emission to the atmosphere or direct application (e.g. by smelting, fossil

51   energy consumption and soil fertilization). Lead is toxic to living organisms even at low doses

52   (World Health Organization et al., 1996). Zinc and Cu are micro-nutrients required in biochemical

53   reactions, but their excessive concentrations lead to toxicity (World Health Organization et al.,

54   1996). In soils, distinguishing between the natural and anthropogenic origins of Pb, Zn and Cu is

55   still a challenge as pedogenetic processes redistribute metals within soil profiles and alter their

56   speciation (Legros, 2007; Semlali et al., 2001). Yet, the distinction is essential for tracing the

57   source of contamination and transfer in soils, and for identifying the potential risks of increased

58   anthropogenic metal transfer in the environment and associated remediation plans.

59   Since the 1990s, Pb isotopes have proved to be powerful tracers of Pb contamination related to

60   gasoline emissions (Erel et al., 1997; Luck and Ben Othman, 2002a; von Storch et al., 2003) and

61   to emissions from industrial areas (Cloquet et al., 2006; Jeon et al., 2017; Wen et al., 2015).

62 Furthermore, Pb isotopes have been used for tracing the transport and redistribution of Pb in the

63 atmosphere (Desenfant et al., 2006; Hamelin et al., 1997; Shotyk et al., 2002; Véron et al., 1999;

64 Weiss et al., 2002). More recently, Cu and Zn isotopes were used to link increased metal

65 concentrations in soils or sediments to the emissions of metallurgic plants (Araújo et al., 2018;

66 Bigalke et al., 2010a; Juillot et al., 2011; Kříbek et al., 2018; Mihaljevič et al., 2018; Sivry et al.,

67 2008; Sonke et al., 2008; Thapalia et al., 2010), or for sourcing metal particles from mining and

68 tailing sites (Borrok et al., 2009; Kimball et al., 2009; Song et al., 2016; Viers et al., 2018).

69 Anthropogenic Cu and Zn isotope tracing relies on large isotopic fractionation (Mattielli et al.,

70 2009; Ochoa Gonzalez and Weiss, 2015; Shiel et al., 2010; Wiederhold, 2015) created during high-

71 temperature industrial processes (e.g., smelting) generating particles emitted to the atmosphere,

72 that are enriched in light isotopes and distinct from the isotopic signatures of soil and from any

73 potential small isotopic fraction induced by natural effects.

74 Most of the above-mentioned studies were conducted on soils near active Zn or Cu smelters with

75 ongoing emissions and only a few focused on long-abandoned contaminated sites (Juillot et al.,

76 2011; Sivry et al., 2008; Sonke et al., 2008). Understanding the fate of historical contamination is

77 challenging because it requires considering the effect of pedogenesis on metal cycling. It has been

78 shown that pedogenetic processes alter Zn and Cu isotopic signatures through post-deposition

79 fractionation (Juillot et al., 2011; Šillerová et al., 2017; Weiss et al., 2008) that with time, may

80 compromise the identification of metal-sources. This post-deposition fractionation is caused by

81 plant uptake of Zn and Cu depleting the soil in light isotopes (Aucour et al., 2015; Jouvin et al.,

82 2012; Viers et al., 2007; Weinstein et al., 2011) and by metal-sorption to soil particles such as Fe-

83 Mn oxides (Balistrieri et al., 2008; Bigalke et al., 2011; Bryan et al., 2015; Juillot et al., 2008;

84 Pokrovsky et al., 2008, 2005) or organic matter (Jouvin et al., 2009; Opfergelt et al., 2017) favoring

85 heavy isotope enrichments in soils.

86 In the 19th century, The Marseilleveyre Massif (Marseilles, France) was home to numerous

87 heavy industries, that have left derelict sites. While the area is now enclosed in the Calanques

88 National Park and is highly protected, it was found to be extensively impacted by these activities

89 (Daumalin and Raveux, 2016). The site of a former Pb-Ag smelter, located in the Escalette

90 Calanque, west of the massif, is particularly appropriate for studying the fate of a historical metal

91 contamination (Figure 1 and S1). It processed argentiferous galena ores from 1851 to 1925 by

92 pyrometallurgical processes and generated massive dumps of Pb and Zn-rich slags and

93 atmospheric emissions of highly metal-concentrated particles. Previous investigations (Affholder

94 et al., 2013; Testiati et al., 2013) showed that soil metal and metalloid concentrations (i.e. Pb, Sb,

95 Zn, Cd and Cu) in the immediate vicinity of the smelter are well above the values of the local

96 biogeochemical background (Austruy et al., 2016). However, no further investigations were

97 performed to evaluate the anthropogenic origin of the metals in more distant soils, or to identify a

98 possible vertical contamination along the soil profile.

99

100 In this study we combined elemental and isotopic Pb, Zn and Cu measurements with X-ray

101 Absorption Spectroscopy (XAS for Zn) analyses to: (i) characterize the isotopic signatures of the

102 pollution originating from the historical Escalette smelter ; (ii) determine whether the Cu

103 concentrations in soils result from galena ore processing or represent natural occurrences; (iii)

104 assess the extent of the vertical transfer of the contamination in a selection of soils of the Calanques

105 National Park located along a transect of increasing distance from the smelter.

106   The Escalette smelter did not process Cu. However, significant amounts of Cu can be present in

107   galena ores, as Cu can substitute into the crystal lattice e.g. (George et al., 2015). Thus, we decided

108   to use Cu isotopes to investigate whether traces of anthropogenic Cu could have been generated

109   during the smelting of galena and whether they could be detected in the surrounding soils.

110   Coupling Zn and Cu isotopes with Pb isotopes that are not affected by isotopic fractionation in

111   soils could help clarify the source of Zn and Cu if the signatures of these elements are too

112   compromised; this is especially the case in subsurface horizons where the pedogenetic processes

113   are the most effective. Furthermore, combining Zn isotopic signatures with Zn-speciation in soils

114   by XAS measurements could shed light on the possible alteration of Zn by pedogenetic processes

115   and/or on the transformation of Zn-bearing phases in soils. This method has proved to be efficient

116   for investigating the cycling of anthropogenic Zn in a soil-plant system (Aucour et al., 2015; Juillot

117   et al., 2011). Such a combination of analytical tools with multi-isotope systems was proposed by

118   Wiederhold (Wiederhold, 2015). To our knowledge, a combination of Pb, Zn and Cu isotopes has

119   been attempted in only one study dedicated to sourcing of urban aerosols (Souto-Oliveira et al.,

120   2018), and it has never been used for soil studies nor in combination with XAS measurements.

121

122   **<u>Material and methods</u>**

123   1.   <u>Smelter samples</u>

124   The Escalette smelter produced PbO and $Ag_{(s)}$ by roasting PbS ores before casting under oxidic

125   conditions at $\sim$ 1100°C, and separation of Pb and Ag. A detailed description of the

126   pyrometallurgical process can be found in Carlier et al. (2010). We collected eight slags resulting

127   from the smelting process along a solid reddish deposit located behind the smelter (Table S1 (c,

128   d)).

129 Grey coatings that had accumulated on the walls of the remaining creeping chimney (ca 300 m-

130 long) were sampled at both ends (i.e. close to the furnace and close to the exit) and in shielded

131 parts not exposed to external climatic conditions. Sampling of true emitted particles was

132 impossible since the smelter has been decommissioned. Considering that the chimney was not

133 equipped with any kind of particle-filtering system, we postulated that the chemical and isotopic

134 compositions of the sample collected at the top end of the chimney were the closest to those of the

135 metals emitted into the atmosphere and to those deposited onto the soils of the surrounding area.

136 Thus, it can be used as a proxy for the material deposited at the surface of the soils in the vicinity

137 of the smelter.

138

139 2. <u>Soil samples</u>

140 We selected five soil profiles along a 7-km NW-SE transect (Figure 1 and S1) of increasing

141 distance from the former smelter, and downwind of the dominant and most powerful wind (NW-

142 SE). These soils were developed on a marine limestone parent material of Cretaceous age, with

143 low metal concentrations (Text S1). The surrounding vegetation is typical of the Mediterranean

144 area (Affholder et al., 2013; Testiati et al., 2013).

145 These five soil profiles (S1, S2, S3, S4 and S5), labelled in order of increasing distance from the

146 smelter, were sampled and described according to the soil horizons. They were selected because

147 of their similar morphological and physico-chemical characteristics to ensure that different soil

148 properties and/or pedogenetic processes did not introduce any bias in the metal-distribution. They

149 are Colluviosols (Baize et al., 2009) or Leptosols (colluvic) (FAO, 2006) with a near neutral pH

150 of 8, an average organic carbon content of 37.3 g kg^{-1}and a mean CaCO$_3$content of 247 g kg^{-1}. All

151 the profiles presented a loose and permeable stone/gravel layer of several centimeters resulting

152 from colluvial movements and set above the usual organic litter and A horizon. X-Ray Diffraction

153 results and physico-chemical characteristics of the samples, determined by the Laboratoire

154 d'Analyse des Sols (LAS) at Arras (INRA, France) are available in SI (Table S1a, S1b).

155

156   3. <u>Total concentrations and isotopic analyses</u>

157   Total concentrations and isotopic analyses were performed on the bulk soils, slags, and chimney

158 coatings. All soil samples were air dried and sieved to < 2mm. They were further crushed to a fine

159 powder in a mechanical agate mortar. For total metal concentrations and isotopic analyses, 150

160 mg of soil sample powder were weighed and calcined at 450°C for 4 hours to eliminate organic

161 matter, then dissolved using a mixture of concentrated HNO_3-HF-HCl at 130°C. Reagents were

162 either distilled acids (HNO_3, HCl) or Seastar© quality (HF). Slags and chimney coatings were

163 ground to a fine powder in an agate mortar and 50 mg of material was totally dissolved using 5 ml

164 of *aqua regia* at 130°C.

165 After digestion, total Pb, Zn and Cu concentrations were measured in solution using a PerkinElmer

166 Nexion 300X Q-ICP-MS.

167   For isotopic analyses, Cu, Zn and Pb were separated and purified using ion exchange

168 chromatography. Copper and Zn were separated and purified using an anionic resin (AG-MP1,

169 100-200 mesh, chloride form), following the procedure published in Maréchal et al. (1999). Lead

170 was separated using an anionic resin (AG1-X8, 100-200 mesh) following the procedure published

171 in (Fekiacova et al., 2007; Lugmair and Galer, 1992).

172   Measurements of Pb, Zn and Cu isotopic compositions were carried out at CEREGE using a

173 Thermo Fisher Scientific Neptune[Plus] Multi-Collector Inductively Coupled Plasma Mass

174 Spectrometer (MC-ICP-MS).

175 ^{208}Pb, ^{207}Pb, ^{206}Pb, ^{204}Pb isotopes corrected for instrumental blanks and mass bias fractionation were

176 measured and are reported as isotope ratios for Pb and as δ notation (per-mil) for Zn (1) and Cu

177 (2) relative to the IRMM-3702 Zn isotopic standard and the AES633 Cu isotopic standard.

178 $$(1) \quad \delta^{66}Zn = \left(\frac{\left(\frac{66Zn}{64Zn}\right)Sample}{\left(\frac{66Zn}{64Zn}\right)IRMM3702} - 1 \right) * 1000$$

179 $$(2) \quad \delta^{65}Cu = \left(\frac{\left(\frac{65Cu}{63Cu}\right)Sample}{\left(\frac{65Cu}{63Cu}\right)AES633} - 1 \right) * 1000$$

180 All data cited in the present paper are expressed relative to the IRMM-3702 standard for Zn and to

181 the AES-633 standard for Cu. In order to compare our data with data from the literature expressed

182 versus the no longer commercially available JMC-37049L (Zn) and NIST-976 (Cu) standards, the

183 following equations were used (Sossi et al., 2015) .

184 $\delta^{66}Zn_{IRMM3702} = \delta^{66}Zn_{JMC37049L}$ - 0.3 ± 0.02 ‰

185 $\delta^{65}Cu_{AES633} = \delta^{65}Cu_{NIST976}$ + 0.01 ± 0.05 ‰

186 For $\delta^{66}Zn$ and $\delta^{65}Cu$, three measurements of each sample digestion were made and expressed as

187 the average value of the three measurements; their repeatability is expressed as two standard

188 deviations (2SD). Seven samples (i.e. all surface horizons of the soils from S1 to S5 and the

189 chimney coatings, top and bottom) were duplicated by conducting a second sample preparation

190 (digestion, column separation and analyses). Reproducibility of the replicated analyses was

191 determined using ANOVA and presented as 2SD. Accuracy was controlled by processing the

192 USGS reference material NOD-P-1 (Manganese nodule) with each batch of samples and

193 reproducibility was calculated on the basis of 6 full replicates using the ANOVA procedure

194 (Addinsoft, 2016). This material is well characterized for Zn (0.55 ±0.08‰; 0.48 ±0.09‰) and

195 Cu (0.36 ±0.08‰; 0.47 ±0.08 isotopic compositions (Bigalke et al., 2010b; Chapman et al., 2006).

196 The mean Zn ($\delta^{66}Zn$IRMM-3702: 0.53 ±0.08 ‰) and Cu ($\delta^{65}Cu$AES-633: 0.45 ± 0.08‰) isotopic

197 compositions of NODP1 obtained during this study agree with previously published data (Bigalke

198 et al., 2010b; Chapman et al., 2006). In addition to the Mn-nodule reference material, soil standards

199 (e.g. GBW07402 from the National Research Centre of Geoanalysis, Beijing, China, TILL-1 from

200 the CANMET Mining and Mineral Sciences Laboratories, Ottawa, Canada) were also processed

201 during this study. Their δ^{66}ZnIRMM-3702 and δ^{65}CuAES-633 isotopic compositions were

202 measured at 0.01 ±0.07‰. However, these results could not be compared to the literature as no

203 values have been published for these standards so far.

204 Copper and Zn chromatographic separation yields of processed samples were measured at 100%

205 ±10%. A further indicator of data quality is the strong correlation between δ^{66}Zn and δ^{67}Zn that

206 matches mass-dependent fractionation processes as specified in (Maréchal et al., 1999) (Figure

207 S2).

208 For Pb isotopes, one measurement was carried out per sample digestion. The repeatability of

209 analyses was estimated from multiple measurements of the bracketing standard NBS981 and is

210 expressed as two standard deviations (2SD).

211 More information on the procedure can be found in SI (Text S2).

212

213   4. <u>EXAFS spectra acquisition and analysis</u>

214   Zinc K-edge X-ray absorption spectra were recorded on samples of the chimney coatings (top)

215 and the surface horizons of S1 and S5 at the ESRF (Grenoble, France) on the BM30B (FAME)

216 beamline. Spectra were measured at liquid helium temperature and in fluorescence mode with a

217 30-element solid state Ge detector. Normalization and data reduction were performed according

218 to standard methods (Doelsch et al., 2006) using Athena software (Ravel and Newville, 2005). A

219 library of Zn reference compound spectra, described elsewhere (Formentini et al., 2017; Legros et

220   al., 2017) was used to identify Zn species in the samples. Details on the fitting procedure and results

221   are given in SI (Text S3, Figure S3 (a, b) and Table S2).

222

223   **Results and discussion**

224   1. **Characterization of slags and grey coatings originating from the former smelter**

225   The Escalette smelter processed various sources of Pb-ores during its exploitation (Daumalin

226   and Raveux, 2016). This variability of sources can impact the isotopic signatures of the volatile

227   and residual phases formed during the smelter process. Moreover, high temperature processes are

228   also known to induce large isotopic fractionation, particularly for Zn.

229   The Pb isotopic compositions of the sampled slags ranged from 2.0759 to 2.0999 and from

230   0.8371 to 0.8529, for $^{208}Pb/^{206}Pb$ and $^{207}Pb/^{206}Pb$ ratios, respectively (Table S1c). As Pb isotopes do not

231   fractionate during the smelting of Pb-Zn ores (Cui and Wu, 2011; Shiel et al., 2010), this

232   heterogeneity reflects the isotopic variability of the ores used during operation of the smelter

233   (Daumalin and Raveux, 2016). By comparing historical reports of the smelter production and a

234   published compilation of the Pb isotopic signature of the main ores (Stos-Gale et al., 1995), two

235   Pb-Ag ores were identified as the origin of these slags: one from the Tuviois ore district (Sardinia,

236   Italy) and the other from the Murcia Mazzaron district (Spain), that is consistent with the historical

237   data found in (Daumalin and Raveux, 2016). The chimney recorded the isotopic signatures of all

238   the processed ores, thus yielding an average Pb isotopic signature typical of the smelter emissions

239   and characterized by values of 2.0924 and 0.8471, for $^{208}Pb^{206}Pb$ and $^{207}Pb^{206}Pb$, respectively (Table

240   S1c).

241   Zinc and Cu isotopic compositions of slags and chimney coatings are presented in Figure 3 (b,

242   c) and Table S1 (c, d). Zinc isotopic composition of the slags, ranged from -0.36 ±0.01 ‰ to -0.14

11

243   ±0.05‰ (n=8), was heavier than that of the chimney coatings. Grey deposits collected in the

244   chimney were enriched in light isotopes: -0.70 ±0.04 ‰ (top sample used as a proxy for the emitted

245   particles, close to the chimney exit) and -0.26 ±0.09 ‰ (bottom, close to the furnace) that is

246   consistent with previously published values for Zn or Cu smelters (Bigalke et al., 2010a; Mattielli

247   et al., 2009; Sonke et al., 2008).

248   Previous studies demonstrated the enrichment of dust particles in light Zn isotopes resulting

249   from Rayleigh-type isotope fractionation (Bigalke et al., 2010a; Mattielli et al., 2009; Shiel et al.,

250   2010; Yin et al., 2016). This mechanism was also active during the Escalette smelting process and

251   produced chimney deposits, enriched in light isotopes. Conversely, residual slags were enriched

252   in heavy isotopes. Yet, the Rayleigh distillation did not produce slags with the same $\delta^{66}Zn$ value as

253   we measured slight variations in the $\delta^{66}Zn$ values of these samples. These variations could reflect

254   the isotopic variability of the galena ores used throughout 74 years of activity. This has also been

255   suggested by other authors (Ochoa Gonzalez and Weiss, 2015) who found that in the combustion

256   process of coal-fired power plants, Zn isotopic signatures of the by-products depended on those of

257   the feed materials. Thus, Zn isotopic signatures of slags were first impacted by the isotopic

258   variability of the parental ores and secondly by the Rayleigh distillation during the smelting.

259   The copper isotopic signature of the collected coatings varied from -0.22 ±0.04 ‰ (top) to -0.46

260   ±0.01 ‰ (bottom). Slags showed a larger range of $\delta^{65}Cu$ values than those observed for Zn isotopes,

261   varying from -1.70 ±0.01‰ to 0.26 ±0.02 ‰ (n=8) (Figure 3c, Table S1c, Table S1d). $\delta^{65}Cu$ values

262   of five out of eight slags were heavier (-0.11 ±0.1‰ to 0.26 ±0.02‰) than the chimney coating

263   signature (-0.22 ±0.04 ‰ (top)). However, three slags displayed a lighter isotopic enrichment (-

264   1.08 ±0.02 ‰; -1.70 ±0.01 ‰; -1.34 ±0.03 ‰) than the chimney coatings (Table S1d).

265   Previous studies showed that Cu is not affected by Rayleigh distillation (Bigalke et al., 2010a;

266   Gale et al., 1999) even in Cu smelters, since the Cu isotopic signatures of ash and slags are similar.

267   The volatilization temperature of Cu is higher than that of Zn (T°$_{volatilization}$: 2595°C and 907°C,

268   respectively). The smelting process temperature at the Escalette smelter varied between 1000 and

269   1150°C (Carlier et al., 2010), thus allowing volatilization for Zn, but not for Cu. We thus

270   hypothesize that the Cu isotopic heterogeneity found in slags mainly resulted from inputs of

271   various galena-ores rather than from an isotopic distillation. No data are available for δ^{65}Cu values

272   in galena ores to confirm this hypothesis, but Cu-S bearing ores (i.e. chalcopyrite and enargite),

273   that are chemically close to the Pb-S (galena) ores processed by the smelter, display δ^{65}Cu values

274   ranging from -1‰ to 1‰ (Mathur et al., 2009) that fit our measurements.

275   We measured different isotopic compositions at the bottom and the top of the chimney (Figure

276   3b, Table S1c). Copper and Zn isotopic signatures of the bottom sample (δ^{65}Cu: -0.46 ±0.01 ‰;

277   δ^{66}Zn: -0.26 ±0.09 ‰) were close to those measured for slags while the top sample was enriched

278   in light Zn isotope (-0.70 ±0.04 ‰), and heavy Cu isotope (-0.22 ±0.04 ‰). We propose therefore

279   that the Cu and Zn isotopic signatures of the chimney bottom sample are close to those of the

280   processed ores like the slags; while in the top sample, isotopic signatures were affected by Rayleigh

281   distillation (for Zn) and equilibrium fractionation (for Cu) that occurred during transport in the

282   vapor phase. A decrease in the plume temperature and condensation of particles during the vapor

283   phase travelling as observed by (Ochoa Gonzalez and Weiss, 2015) in bottom and flying ash

284   samples from a coal power plant could explain the differences in metal concentrations between the

285   two extremities of the chimney. Like other smelters in the area at that time, the Escalette smelter

286   is characterized by a long sub-horizontal conduit, built on the ground, and creeping up the hill

287   along the ridge rather than by the short, vertical chimneys as found in modern smelters. Thus,

288 interactions of Zn and Cu during transport in the vapor phase were maximized causing an

289 enrichment in light Zn isotope and an enrichment in heavy Cu isotope (Balistrieri et al., 2008;

290 Pokrovsky et al., 2008).

291

292 **2. <u>Assessing the extent of the soil contamination</u>**

293 <u>Elemental concentrations: highlighting soil surface contamination.</u>

294   Trace metal concentrations in the soil profiles (Figure 2a, b, c and Table S1c) were studied to

295 determine the horizontal extent of metal contamination in the vicinity of the Escalette smelter.

296 Surface horizons of the S1, S2, and S3 profiles were clearly affected by atmospheric deposition of

297 metal-rich particles with Pb and Zn concentrations decreasing with increasing distance from the

298 smelter and metal levels in the S1 A horizon up to 121x (Pb) and 14x (Zn) those found in the deep

299 horizon of the more distant soil (S5 C) (table S1c).

300   For all the studied soils, the surface horizons showed higher Pb, Zn, and Cu concentrations than

301 deeper horizons except for S5 that had the lowest trace metal concentrations in the A horizons. All

302 Zn and Pb concentrations were well above the values measured in five unpolluted local soils

303 developed on calcareous parent materials (Austruy et al., 2016), both for the A topsoil (up to 22-

304 fold for Zn and 39-fold for Pb) and for the subsoils (up to 3-fold for Zn and Pb). In S5, Zn

305 concentrations were higher than those for natural calcareous soils in both surface (27 to 64 mg kg

306 $^{-1}$(Austruy et al., 2016)) and deep horizons (19 to 59 mg kg^{-1}(Austruy et al., 2016)). However, Pb

307 concentrations were lower than those estimated by (Austruy et al., 2016) both for surface (20 to

308 78 mg kg^{-1}) and deep horizons (9 to 42 mg kg^{-1}).

309   In all soils, Cu concentrations were low and close to geogenic values ranging from 4 mg kg^{-1} to

310 17 mg kg^{-1} (Austruy et al., 2016) compared to Zn and Pb (Figure 2c). However, S1 displayed

311   concentrations ~2.5x higher than S5 indicating a small potential contamination by smelter

312   emissions. Soils displayed more homogenous Cu concentrations with a smaller depth-induced

313   decrease, that was most likely due to initially lower Cu concentrations in the parental limestone

314   and to a low concentration in the source galena, thus in smelter emissions.

315   Although S2 was closer to the smelter than S3 (Figure S1b), Zn, Pb, and Cu concentrations were

316   lower. This could be related to the fact that S2 was obscured from direct line of sight by a

317   calcareous cliff that may have limited the deposition of metal-bearing airborne particles even with

318   NNW winds that can reach up to 110 km h^{-1}.

319   High trace metal concentrations in surface horizons decreasing with depth are similar to patterns

320   observed in uncontaminated soils (Legros, 2007). Furthermore, higher trace metal concentrations

321   in deep horizons compared to other soils in the area could originate from a higher pedogeochemical

322   background. Local variations in the natural pedo-geochemical background can be determined from

323   the relationship between total Fe and the trace metals and can provide information about a potential

324   trace metal contamination (Baize and Sterckeman, 2001). In our soils, the relationship between

325   total Fe and trace metals made it possible to distinguish between (i) a group of deep horizons

326   having low trace metal concentrations and (ii) a group of surface horizons, with a high trace metal

327   content for relatively low Fe concentrations. This approach revealed the horizontal extent of trace

328   metal contamination of surface horizons in the Escalette area, but did not inform on the potential

329   transfers of anthropogenic metals down the profiles and/or on the source contributions.

330

331   **3. Isotopic signatures: tracing the smelter contamination in soil profiles**

332   3.1 Lead

333   The surface horizons of all profiles showed Pb isotopic compositions similar to those of the

334   chimney coatings and the slags, indicating that lead contamination originated from smelter

335   emissions. In a $^{208}Pb/^{206}Pb$ vs $^{207}Pb/^{206}Pb$ plot (Figure 4a), soils and chimney coatings lay along a linear

336   trend corresponding to a mixing line between a radiogenic end-member (i.e. the emitted

337   anthropogenic Pb), and an uncontaminated end-member characterized by a lower radiogenic Pb

338   signature (i.e. the local pedogeochemical background) found in the S5 deepest horizon.

339   Lead isotopic ratios of the slags plotted out this $^{208}Pb/^{206}Pb$ vs $^{207}Pb/^{206}Pb$ mixing line (Figure 4a) and

340   demonstrate that slag-generated dust did not contribute to the soil contamination. Moreover,

341   considering the local topography and the fact that these slags appeared as a solid unaltered material,

342   it is unlikely that slag-related dust contaminated soils located at the top of the slopes. This

343   observation supports the hypothesis that Pb contamination in soils was solely caused by the metal-

344   rich particles emitted by the smelter. Furthermore, the chimney signature reflects the average

345   composition of all the isotopic compositions of galena ores processed over time (Figure 3a and

346   Figure 4a).

347   The limited variation of $^{208}Pb/^{206}Pb$ ratios with depth (Figure 3a) or the soil profile distribution on

348   the mixing line (Figure 4a), indicates that (i) Pb contamination affected all soils from S1 to S5 (ii)

349   Pb concentrations in soils resulted from two lead sources and (iii), anthropogenic Pb was

350   transferred towards depth.

351   In Figure 4a the S5 A horizon lies slightly off the mixing line, indicating that this sample received

352   a contribution from another lead source other than the smelter, e.g. urban aerosols or modern

353   industrial sources. Three-component mixing for this sample can also be identified in a $^{208}Pb/^{204}Pb$ vs

354    $^{206}Pb/^{204}Pb$ plot (Figure 4b) as suggested by (Ellam, 2010). This source was not observed in other

355   soils because of the dominant lead signature from the smelter particles. We hypothesize that this

16

356   source may be representative of the atmospheric aerosols emitted by the combustion of fossil

357   energy (i.e. road traffic in Marseilles) after the closing of the smelter.

358   Reconstruction of the lead isotopic signature of French (northern and southern) atmospheric

359   aerosols since the 1980s, based on previously published data (Luck and Ben Othman, 2002b;

360   Maring et al., 1987; Véron et al., 1999), produced a mixing line (r^2 = 0.95; p value =$1.40E^{-19}$) that

361   did not intersect our S5 A horizon sample, but instead drove it away from the two end-member

362   mixture (Figure S4).

363   <u>3.2 Zinc</u>

364   Zinc isotopic signatures of the smelter samples (chimney) and the soil samples were different

365   (Figure 3b). The impact of light Zn-rich particles originating from the smelter could nonetheless

366   be detected in the surface horizons.

367   Soil surface horizons from S1 to S4 showed $\delta^{66}Zn$ values ranging from -0.24 ±0.05 ‰ to -0.43

368   ±0.06‰ (Table S1c, Figure 3b). The surface horizon of S5 had the heaviest Zn isotopic signature

369   (-0.14 ±0.06‰ Figure 3b), that remained constant along the entire profile.

370   Isotope studies carried out on peat core sediments (Sonke et al., 2008) or on soils collected near a

371   Zn or Cu smelter (Bigalke et al., 2010a; Juillot et al., 2011), revealed a similar enrichment in light

372   isotopes in the sediment/soil surface samples compared to those measured in the chimney stacks

373   or smelter dust. However, these studies also noted discrepancies between Zn isotopic compositions

374   of the smelter emissions and those of the sediment/soils. The discrepancy was explained by either

375   mixing of the ash/dust signal with other emissions from different subunits of the smelter (Bigalke

376   et al., 2010a; Juillot et al., 2011) or by post-depositional fractionation (Juillot et al., 2011) that

377   induced direct heavy enrichment in soils by Zn-sorption onto oxides and OM (Bryan et al., 2015;

378   Guinoiseau et al., 2016; Jouvin et al., 2009; Juillot et al., 2008; Pokrovsky et al., 2005) or depletion

379   in light isotopes by plant uptake (Aucour et al., 2015; Jouvin et al., 2012; Viers et al., 2007). This

380   hypothesis was supported by other authors (Mattielli et al., 2009) who found a perfect match

381   between Zn isotopic composition of the chimney dust and particles collected on dry plate rather

382   than environmental (soil) samples, thus preventing any interactions with soil particles or plant

383   uptake. Thus, the enrichment in heavy Zn isotopes in surface horizons of the studied soils could

384   be explained by the direct (i.e. sorption) or the indirect (i.e. plant uptake) effect of post-deposition

385   fractionation processes.

386   Soil profiles S1, S2, and S3 displayed isotopic variations with depth, up to $\Delta^{66}Zn_{\text{S3 A horizon-S3 S horizon}}$ =

387   0.21 ‰ in S3 soil, and an increase in the $\delta^{66}Zn$ values down to ~ 0.2 m (Figure 3b). $\delta^{66}Zn$ values of

388   the deepest horizons of S1, S2, S3, and S4 were close to the isotopic signature of S5 and indicated

389   that Zn contamination may have been limited at depth. Homogeneous Zn concentrations and $\delta^{66}Zn$

390   values in the S5 profile were (i) clearly distinct from those of the chimney and of the other soils,

391   and (ii) fell within the range of previously published values for non-contaminated soils or

392   continental rock parental material (-0.19 to 0.06 ‰) (Juillot et al., 2011; Pichat et al., 2003; Sonke

393   et al., 2008; Wilkinson et al., 2005). Thus, we propose that the $\delta^{66}Zn$ value in S5 (~ -0.16 ‰)

394   reflects the Zn isotopic signature of the local uncontaminated weathered parent material for the

395   studied soil.

396

397   <u>3.3 Copper</u>

398   Given the proximity of S1, S2, and S3 to the chimney, a significant contribution of particle

399   deposition on the Cu isotopic signatures in these soils was expected, especially for S1 where the

400   Cu concentration was slightly higher in the A horizon (Figure 2c). However, (i) Cu isotopic

401 signatures in the A horizons of S1 and S5 are similar (Figure 3c), and (ii) they did not reveal any

402 similarities between soil surface and chimney coating unlike for Pb and Zn isotopes (Figure 3c).

403 Except for S4, all profiles showed a similar vertical distribution, with an increasing light isotope

404 contribution at depth as observed in (Bigalke et al., 2011; Mihaljevič et al., 2018) for natural soils.

405 $\delta^{65}Cu$ values in deep horizons ranged from -0.30 ±0.04 ‰ to -0.73 ±0.03 ‰, values that are within

406 the range of $\delta^{65}Cu$ values measured in unpolluted soils, (-0.9 to 0.45 ‰ (Bigalke et al., 2011;

407 Fekiacova et al., 2015; Kříbek et al., 2018).

408 We conclude that anthropogenic inputs of Cu from the smelter were negligible and observed Cu

409 fractionation in the soil profiles was produced by pedogenetic processes. Two major processes are

410 known to impact natural Cu isotopic signatures in soils: plant recycling (Jouvin et al., 2012;

411 Weinstein et al., 2011) and interactions with solid mineral particles and/or solid organic matter

412 (Balistrieri et al., 2008; Bigalke et al., 2011; Pokrovsky et al., 2008). These interactions cause

413 direct (preferential sorption) and indirect (depletion of light isotopes by plant uptake) heavy

414 isotope enrichment in soils. We propose that Cu concentrations in the soils were inherited from

415 the parent material and higher Cu concentrations in the surface horizons resulted from Cu

416 complexation to the organic matter. A ^{65}Cu enrichment observed in the surface horizons

417 corroborates this hypothesis.

418

419 **4. Long-term fate of anthropogenic Pb and Zn in soils.**

420 Emissions from the Escalette smelter and contamination started 167 years ago and lasted 74

421 years. Thus, the Escalette site provides a unique place to unravel the long-term fate of

422 anthropogenic Pb and Zn in terms of remobilization/redistribution within the impacted soils.

423

4.1 Lead

425   The limited vertical variation of $^{208}Pb/^{206}Pb$ ratios (Figure 3a) indicated that anthropogenic Pb,

426   characterized by a high $^{208}Pb/^{206}Pb$ ratio (Table S1c), was transferred to depth from S1 to S4. Soluble

427   transport of Pb in carbonated soil is limited because of the preferential precipitation of Pb as

428   carbonates (cerussite, hydrocerussite or pyromorphite) at pH > 5.2 (Gee et al., 1997; Yanful et al.,

429   1988). The pH of all studied soils ranged from 7.9 to 8.3 suggesting possible Pb carbonate

430   precipitation, although no Pb carbonate was detected by XRD (probably due to concentrations

431   below the detection limit). Considering the high distribution coefficient (Kd) of Pb for OM and

432   Fe-oxides in poorly developed carbonated soils (Dumat et al., 2001; Lafuente et al., 2008), Pb is

433   likely to occur as complexes with organic matter and soil minerals in the surface horizons of the

434   studied soils. We hypothesized that Pb redistribution by colluvial processes could explain the

435   results. However, erosion of upslope-contaminated-material and accumulation of eroded material

436   downslope should be reflected by (i) Pb and Zn concentration peaks in subsurface horizons of

437   downslope profiles, and (ii) abrupt changes in the Zn isotopic signatures of intermediate horizons

438   toward light values caused by the integration of smelter-derived particles characterized by light

439     $\delta^{66}Zn$ values. Since none of these effects were observed, we concluded that colluvial processes

440   were not responsible for anthropogenic Pb migration.

441   Using a mixing model between two end-members (Figure 4a and 5) represented by the deepest

442   horizon of S5 (C) and the chimney coating (top) and based on the calculation proposed by (Phillips

443   and Gregg, 2003), we can estimate the contribution of anthropogenic Pb to the total Pb pool in

444   soils. We found that Pb-rich particles from the smelter (Figure 5, Table S3) account for at least

445   91% of the total Pb pool measured in soil surface horizons from S1 to S4. The deepest soil horizons

446   show the same trend with an anthropogenic Pb contribution estimated between 65-78% from S1

447   to S4.

448   The A horizon of S5 plotted out of the mixing line (Figure 4a and Figure 5) and the ^{208}Pb/^{204}Pb vs

449   ^{206}Pb/^{204}Pb isotope plot confirmed the contribution of a third source of Pb in this sample (Figure 4b).

450   Thus, we used the Isosource program (Phillips and Gregg, 2003), provided by the Environmental

451   Protection Agency, to calculate contributions of different Pb sources in a three end-member system

452   (smelter, geogenic, atmospheric). The third Pb source considered in the system was urban aerosol,

453   with values of ^{208}Pb/^{206}Pb = 2.1367 and ^{207}Pb/^{206}Pb = 0.8944, approximated by the Pb signature of

454   Marseilles aerosols in 1987 (Maring et al., 1987).

455   According to these calculations, in S5 (the most distant soil from the smelter), the contribution of

456   smelter-related anthropogenic Pb was best estimated at 39%, geogenic Pb at 42% and atmospheric

457   Pb at 19%. The distributions of all possible contributions that satisfied the isotopic mass balance

458   calculations are presented in (Figure S5, Table S3).

459   This observation indicated that some Pb-rich particles from the smelter travelled up to 7 km SE.

460   However, because of a lower concentration of the smelter-derived particles, Pb isotopic signature

461   of S5 was significantly disturbed by inputs of atmospheric particles when smelter emissions

462   stopped in 1925. At the other sites, the impact of atmospheric particles was not observable, most

463   likely due to a higher content of smelter-derived particles.

464   The anthropogenic Pb contribution to total Pb decreased progressively with depth in all soils,

465   excluding the impact of colluvial processes on Pb distribution in soils as stated above. Based on

466   soil thickness, we calculated Pb penetration rates in soils ranging from 0.27 cm year^{-1} (S1 soil) to

467   0.47 cm year^{-1} (S3 soil) for a lower limit (i.e. calculated since the opening of the smelter, 167 years

468   ago) or 0.48 cm year^{-1} to 0.85 cm year^{-1} in the same soils for the upper limit (i.e. calculated since

469   the decommissioning of the smelter, 93 years ago). As Pb migration has been found to be facilitated

470   by colloidal transport in contaminated soil (Amrhein et al., 1993; Denaix et al., 2001; Grolimund

471   et al., 1996; Grolimund and Borkovec, 2005; Kretzschmar and Schafer, 2005) and because of both

472   low Pb concentrations in the $< 0.2\,\mu$m soluble phase (Gelly et al. *in prep*) and low soil density, we

473   propose that in the soils, this transfer occurred in the particulate form. Furthermore, metal

474   migration could have been enhanced by bioturbation (e.g. (Sterckeman et al., 2000), but we did

475   not observe any evidence of significant worm activity to support this hypothesis.

476

477   <u>4.2 Zinc</u>

478   Zinc contamination was detected using Zn isotopes in all soils except S5. However, vertical

479   variations in δ⁶⁶Zn values indicated that Zn mobility was different from that observed for Pb.

480   Smelter-related Zn, characterized by light δ⁶⁶Zn values (Figure 3b), accumulated within the A and

481   A/C horizons. However, the observed shift towards heavier signatures in the studied soils

482   demonstrates that another process modified the initial anthropogenic Zn signature. This shift could

483   be attributed to (i) Zn adsorption or precipitation on organic matter and Al-Fe-Mn oxides

484   (Balistrieri et al., 2008; Juillot et al., 2008; Pokrovsky et al., 2005), that would promote heavy

485   isotope complexes, or to (ii) plant uptake, that would deplete soil in light isotopes, thus enriching

486   it in heavy ones (Aucour et al., 2015; Jouvin et al., 2012; Viers et al., 2007).

487   EXAFS results support the hypothesis of the transformation of anthropogenic Zn. In S1, Zn

488   speciation could not be fitted by a simple combination of the chimney (anthropogenic contribution)

489   and S5 compositions (natural contribution), indicating a change in the smelter-related Zn

490   speciation after deposition onto the soil (Figure S3b). EXAFS results highlighted the precipitation

491   of a Zn-layered double hydroxide (Zn-LDH) phase which was dominant (~77%, Table S2) in S1

492 topsoil, while in the S5 soil, Zn was mostly sorbed onto Fe and Mn oxides (Table S2). Zn-LDH

493 precipitates have been identified as markers of Zn contamination in calcareous soils (Jacquat et

494 al., 2008; Juillot et al., 2003; Voegelin et al., 2011) or other contaminated soils (Aucour et al.,

495 2015; Voegelin et al., 2005). Zn-LDH precipitation occurs once all sorption sites have been

496 saturated (Luxton et al., 2013) and is kinetically favored over precipitation of Zn-phyllosilicates,

497 although these precipitates are also thermodynamically stable (Voegelin et al., 2005). The

498 availability of Al and Si (Jacquat et al., 2008; Voegelin et al., 2005) and increasing Zn

499 concentrations in soils seem to play a major role in the formation of Zn-LDH. No occurrences of

500 Zn-LDH in Pb and/or Zn smelter exhausts have been reported in the literature. Similarly, we did

501 not detect these compounds in the Escalette chimney (Table S2), most likely indicating

502 unfavorable physico-chemical conditions in the chimney (e.g. more acidic pH).

503   Thus, Zn-LDH formation was considered to have contributed to (i) precipitation of smelter-

504 related Zn in the S1 surface horizon, and (ii) alteration of the Zn isotopic signatures of the emitted

505 particles by favoring heavy isotope complexes. Owing to the similarity in the Zn isotopic signature

506 of the A horizons in S1 to S4, the same process may have occurred in all studied soils.

507   The mixing model calculated for Zn (like the model calculated for Pb) did not show any

508 progressive mixing between the two end-members, but rather highlighted two Zn pools. One pool

509 was represented by the surface horizons of soils from S1 to S4, the second one was represented by

510 the deepest horizons of these soils and by the entire S5 profile (Figure 6). Separation of the Zn

511 pools confirmed that anthropogenic Zn accumulated in surface horizons and that precipitation of

512 the Zn-LDH prevented leaching of Zn towards deeper horizons. Consequently, at depth, Zn is

513 considered to be of geogenic origin (inherited from the parental limestone).

514   Zinc isotopes confirmed that few Zn-rich particles reached S5 as their impact was not recorded by

515   the δ^{66}Zn values, probably because anthropogenic Zn was incorporated in soils through pedogenetic

516   processes as illustrated by EXAFS analyses (Table S2).

517

518   <u>Conclusion</u>

519   We used isotopic analyses to shed light on the behavior and transfer in soils of Pb, Zn, and Cu

520   emitted simultaneously from the Escalette smelter, for 93 years. In contrast to Pb and Zn, Cu

521   isotopes showed no evidence of Cu contamination of the soils in the vicinity of the Escalette

522   smelter.

523   We recovered traces of smelter emissions in the soil surface (Zn-Pb) up to 7 km away from the

524   smelter and at depth (Pb). The vertical mobility of anthropogenic Pb contrasts with previously

525   published data on calcareous soils where Pb was immobilized in surface horizons.

526   In contrast, immobilization of smelter-related Zn within the surface horizons was documented

527   by the shift in δ^{66}Zn values in soils compared to those of the chimney coatings, representing the

528   proxy used for the isotopic signatures of the emitted particles. This is explained by the precipitation

529   of Zn-LDH, typical of Zn-rich environments with near-neutral to slightly basic pH. This form of

530   Zn was different from those observed in the chimney coatings and in S5, indicating that (i)

531   speciation of Zn emitted from the smelter changed after deposition, altering Zn isotopic signatures,

532   and (ii) fewer Zn-rich particles reached S5 and were included in the biogeochemical cycle of Zn

533   through pedogenetic processes.

534   However, the role of vegetation in the anthropogenic Zn cycling at this site needs to be

535   deciphered in future studies. Particularly, *in natura* isotopic measurements could shed light on how

536   the vegetation adapts to anthropogenic metals and incorporates them into its biogeochemical cycle.

537 This work underlines the complementarity of elemental, isotopic, and speciation analyses for

538 tracing and unravelling the fate of historical multi-metal contamination in soils by providing a

539 complementary set of data that highlights the distinctive behavior of trace metals originating from

540 a common industrial source.

541

542

543 Acknowledgement

553 References

554 Addinsoft, 2016. XLSTAT 2016: Data Analysis and Statistical Solution for Microsoft Excel.
555 Affholder, M.-C., Prudent, P., Masotti, V., Coulomb, B., Rabier, J., Nguyen-The, B., Laffont-
556   Schwob, I., 2013. Transfer of metals and metalloids from soil to shoots in wild rosemary
557   (Rosmarinus officinalis L.) growing on a former lead smelter site: Human exposure risk.
558   Sci. Total Environ. 454–455, 219–229. https://doi.org/10.1016/j.scitotenv.2013.02.086
559 Amrhein, C., Mosher, P.A., Strong, J.E., 1993. Colloid-Assisted Transport of Trace Metals in
560   Roadside Soils Receiving Deicing Salts. Soil Sci. Soc. Am. J. 57, 1212.
561   https://doi.org/10.2136/sssaj1993.03615995005700050009x
562 Araújo, D.F., Machado, W., Weiss, D., Mulholland, D.S., Garnier, J., Souto-Oliveira, C.E.,
563   Babinski, M., 2018. Zinc isotopes as tracers of anthropogenic sources and biogeochemical

564 processes in contaminated mangroves. Appl. Geochem. 95, 25–32.
565 https://doi.org/10.1016/j.apgeochem.2018.05.008

566 Aucour, A.-M., Bedell, J.-P., Queyron, M., Magnin, V., Testemale, D., Sarret, G., 2015. Dynamics
567 of Zn in an urban wetland soil–plant system: Coupling isotopic and EXAFS approaches.
568 Geochim. Cosmochim. Acta 160, 55–69. https://doi.org/10.1016/j.gca.2015.03.040

569 Austruy, A., Dron, J., Charbonnier, E., Babaguela, N., Miche, H., Keller, C., Chamaret, P., 2016.
570 Teneurs naturelles et apports anthropiques en éléments traces dans les sols à l'ouest de
571 l'étang de Berre. Etude Gest. Sols 18.

572 Baize, D., Girard, M.-C., others, 2009. Référentiel pédologique 2008. Quae.

573 Baize, D., Sterckeman, T., 2001. Of the necessity of knowledge of the natural pedo-geochemical
574 background content in the evaluation of the contamination of soils by trace elements. Sci.
575 Total Environ. 264, 127–139. https://doi.org/10.1016/S0048-9697(00)00615-X

576 Balistrieri, L.S., Borrok, D.M., Wanty, R.B., Ridley, W.I., 2008. Fractionation of Cu and Zn
577 isotopes during adsorption onto amorphous Fe(III) oxyhydroxide: Experimental mixing of
578 acid rock drainage and ambient river water. Geochim. Cosmochim. Acta 72, 311–328.
579 https://doi.org/10.1016/j.gca.2007.11.013

580 Bigalke, M., Weyer, S., Kobza, J., Wilcke, W., 2010a. Stable Cu and Zn isotope ratios as tracers
581 of sources and transport of Cu and Zn in contaminated soil. Geochim. Cosmochim. Acta
582 74, 6801–6813. https://doi.org/10.1016/j.gca.2010.08.044

583 Bigalke, M., Weyer, S., Kobza, J., Wilcke, W., 2010b. Stable Cu and Zn isotope ratios as tracers
584 of sources and transport of Cu and Zn in contaminated soil. Geochim. Cosmochim. Acta
585 74, 6801–6813. https://doi.org/10.1016/j.gca.2010.08.044

586 Bigalke, M., Weyer, S., Wilcke, W., 2011. Stable Cu isotope fractionation in soils during oxic
587 weathering and podzolization. Geochim. Cosmochim. Acta 75, 3119–3134.
588 https://doi.org/10.1016/j.gca.2011.03.005

589 Borrok, D.M., Wanty, R.B., Ian Ridley, W., Lamothe, P.J., Kimball, B.A., Verplanck, P.L.,
590 Runkel, R.L., 2009. Application of iron and zinc isotopes to track the sources and
591 mechanisms of metal loading in a mountain watershed. Appl. Geochem. 24, 1270–1277.
592 https://doi.org/10.1016/j.apgeochem.2009.03.010

593 Bryan, A.L., Dong, S., Wilkes, E.B., Wasylenki, L.E., 2015. Zinc isotope fractionation during
594 adsorption onto Mn oxyhydroxide at low and high ionic strength. Geochim. Cosmochim.
595 Acta 157, 182–197. https://doi.org/10.1016/j.gca.2015.01.026

596 Carlier, C.M.-L., Ploquin, A., Fluck, P., 2010. Apport de la géochimie et de la pétrologie à la
597 connaissance de la métallurgie primaire du plomb argentifère au Moyen Âge: Les exemples
598 du Mont Lozère (Cévennes) et de Pfaffenloch (Vosges). ArchéoSciences 159–176.
599 https://doi.org/10.4000/archeosciences.2728

600 Chapman, J.B., Mason, T.F.D., Weiss, D.J., Coles, B.J., Wilkinson, J.J., 2006. Chemical
601 Separation and Isotopic Variations of Cu and Zn From Five Geological Reference
602 Materials. Geostand. Geoanalytical Res. 30, 5–16. https://doi.org/10.1111/j.1751-
603 908X.2006.tb00907.x

604 Cloquet, C., Carignan, J., Libourel, G., Sterckeman, T., Perdrix, E., 2006. Tracing Source Pollution
605 in Soils Using Cadmium and Lead Isotopes. Environ. Sci. Technol. 40, 2525–2530.
606 https://doi.org/10.1021/es052232+

607 Cui, J., Wu, X., 2011. AN EXPERIMENTAL INVESTIGATION ON LEAD ISOTOPIC
608 FRACTIONATION DURING METALLURGICAL PROCESSES: Lead isotopic

fractionation during metallurgical processes. Archaeometry 53, 205–214. https://doi.org/10.1111/j.1475-4754.2010.00548.x

Daumalin, X., Raveux, O., 2016. A region scarred by pollution, in: Xavier Daumalin, I.L.-S. (dir. . (Ed.), Es Calanques Industrielles de Marseille et Leurs Pollutions. Une Histoire Au Présent. REF.2C éditions, pp. 131–203.

Denaix, L., Semlali, R.M., Douay, F., 2001. Dissolved and colloidal transport of Cd, Pb, and Zn in a silt loam soil a ected by atmospheric industrial deposition. Environ. Pollut. 10.

Desenfant, F., Veron, A.J., Camoin, G.F., Nyberg, J., 2006. Reconstruction of pollutant lead invasion into the tropical North Atlantic during the twentieth century. Coral Reefs 25, 473–484. https://doi.org/10.1007/s00338-006-0113-x

Doelsch, E., Masion, A., Borschneck, D., Hazemann, J.-L., Saint Macary, H., Bottero, J.-Y., Rose, J., Basile-Doelsch, I., 2006. New Combination of EXAFS Spectroscopy and Density Fractionation for the Speciation of Chromium within an Andosol. Environ. Sci. Technol. 40, 7602–7608. https://doi.org/10.1021/es060906q

Dumat, C., Chiquet, A., Gooddy, D., Aubry, E., Morin, G., Juillot, F., Benedetti, M.F., 2001. Metal ion geochemistry in smelter impacted soils and soil solutions. Bull. Société Géologique Fr. 172, 539–548. https://doi.org/10.2113/172.5.539

Ellam, R.M., 2010. The graphical presentation of lead isotope data for environmental source apportionment. Sci. Total Environ. 408, 3490–3492. https://doi.org/10.1016/j.scitotenv.2010.03.037

Erel, Y., Veron, A., Halicz, L., 1997. Tracing the transport of anthropogenic lead in the atmosphere and in soils using isotopic ratios. Geochim. Cosmochim. Acta 61, 4495–4505. https://doi.org/10.1016/S0016-7037(97)00353-0

FAO (Ed.), 2006. World reference base for soil resources 2006: a framework for international classification, correlation and communication, World soil resources reports. FAO, Rome.

Fekiacova, Z., Abouchami, W., Galer, S.J.G., Garcia, M.O., Hofmann, A.W., 2007. Origin and temporal evolution of Ko'olau Volcano, Hawai'i: Inferences from isotope data on the Ko'olau Scientific Drilling Project (KSDP), the Honolulu Volcanics and ODP Site 843. Earth Planet. Sci. Lett. 261, 65–83. https://doi.org/10.1016/j.epsl.2007.06.005

Fekiacova, Z., Cornu, S., Pichat, S., 2015. Tracing contamination sources in soils with Cu and Zn isotopic ratios. Sci. Total Environ. 517, 96–105. https://doi.org/10.1016/j.scitotenv.2015.02.046

Formentini, T.A., Legros, S., Fernandes, C.V.S., Pinheiro, A., Le Bars, M., Levard, C., Mallmann, F.J.K., da Veiga, M., Doelsch, E., 2017. Radical change of Zn speciation in pig slurry amended soil: Key role of nano-sized sulfide particles. Environ. Pollut. 222, 495–503. https://doi.org/10.1016/j.envpol.2016.11.056

Gale, N.., Woodhead, A.., Stos-Gale, Z.., Walder, A., Bowen, I., 1999. Natural variations detected in the isotopic composition of copper: possible applications to archaeology and geochemistry. Int. J. Mass Spectrom. 184, 1–9. https://doi.org/10.1016/S1387-3806(98)14294-X

Gee, C., Ramsey, M.H., Maskall, J., Thornton, I., 1997. Mineralogy and weathering processes in historical smelting slags and their effect on the mobilisation of lead. J. Geochem. Explor. 58, 249–257. https://doi.org/10.1016/S0375-6742(96)00062-3

George, L., Cook, N.J., Ciobanu, C.L., Wade, B.P., 2015. Trace and minor elements in galena: A reconnaissance LA-ICP-MS study. Am. Mineral. 100, 548–569. https://doi.org/10.2138/am-2015-4862

655 Grolimund, D., Borkovec, M., 2005. Colloid-Facilitated Transport of Strongly Sorbing
656   Contaminants in Natural Porous Media: Mathematical Modeling and Laboratory Column
657   Experiments †. Environ. Sci. Technol. 39, 6378–6386. https://doi.org/10.1021/es050207y
658 Grolimund, D., Borkovec, M., Barmettler, K., Sticher, H., 1996. Colloid-Facilitated Transport of
659   Strongly Sorbing Contaminants in Natural Porous Media: A Laboratory Column Study.
660   Environ. Sci. Technol. 30, 3118–3123. https://doi.org/10.1021/es960246x
661 Guinoiseau, D., Gélabert, A., Moureau, J., Louvat, P., Benedetti, M.F., 2016. Zn Isotope
662   Fractionation during Sorption onto Kaolinite. Environ. Sci. Technol. 50, 1844–1852.
663   https://doi.org/10.1021/acs.est.5b05347
664 Hamelin, B., Ferrand, J.L., Alleman, L., Nicolas, E., Veron, A., 1997. Isotopic evidence of
665   pollutant lead transport from North America to the subtropical North Atlantic gyre.
666   Geochim. Cosmochim. Acta 61, 4423–4428. https://doi.org/10.1016/S0016-
667   7037(97)00242-1
668 Jacquat, O., Voegelin, A., Villard, A., Marcus, M.A., Kretzschmar, R., 2008. Formation of Zn-
669   rich phyllosilicate, Zn-layered double hydroxide and hydrozincite in contaminated
670   calcareous soils. Geochim. Cosmochim. Acta 72, 5037–5054.
671   https://doi.org/10.1016/j.gca.2008.07.024
672 Jeon, S., Kwon, M.J., Yang, J., Lee, S., 2017. Identifying the source of Zn in soils around a Zn
673   smelter using Pb isotope ratios and mineralogical analysis. Sci. Total Environ. 601–602,
674   66–72. https://doi.org/10.1016/j.scitotenv.2017.05.181
675 Jouvin, D., Louvat, P., Juillot, F., Maréchal, C.N., Benedetti, M.F., 2009. Zinc Isotopic
676   Fractionation: Why Organic Matters. Environ. Sci. Technol. 43, 5747–5754.
677   https://doi.org/10.1021/es803012e
678 Jouvin, D., Weiss, D.J., Mason, T.F.M., Bravin, M.N., Louvat, P., Zhao, F., Ferec, F., Hinsinger,
679   P., Benedetti, M.F., 2012. Stable Isotopes of Cu and Zn in Higher Plants: Evidence for Cu
680   Reduction at the Root Surface and Two Conceptual Models for Isotopic Fractionation
681   Processes. Environ. Sci. Technol. 46, 2652–2660. https://doi.org/10.1021/es202587m
682 Juillot, F., Maréchal, C., Morin, G., Jouvin, D., Cacaly, S., Telouk, P., Benedetti, M.F., Ildefonse,
683   P., Sutton, S., Guyot, F., Brown, G.E., 2011. Contrasting isotopic signatures between
684   anthropogenic and geogenic Zn and evidence for post-depositional fractionation processes
685   in smelter-impacted soils from Northern France. Geochim. Cosmochim. Acta 75, 2295–
686   2308. https://doi.org/10.1016/j.gca.2011.02.004
687 Juillot, F., Maréchal, C., Ponthieu, M., Cacaly, S., Morin, G., Benedetti, M., Hazemann, J.L.,
688   Proux, O., Guyot, F., 2008. Zn isotopic fractionation caused by sorption on goethite and 2-
689   Lines ferrihydrite. Geochim. Cosmochim. Acta 72, 4886–4900.
690   https://doi.org/10.1016/j.gca.2008.07.007
691 Juillot, F., Morin, G., Ildefonse, P., Trainor, T.P., Benedetti, M., Galoisy, L., Calas, G., Brown,
692   G.E., 2003. Occurrence of Zn/Al hydrotalcite in smelter-impacted soils from northern
693   France: Evidence from EXAFS spectroscopy and chemical extractions. Am. Mineral. 88,
694   509–526. https://doi.org/10.2138/am-2003-0405
695 Kabata-Pendias, A., 2011. Trace Elements in Soils and Plants, Fourth Edition 33.
696 Kimball, B.E., Mathur, R., Dohnalkova, A.C., Wall, A.J., Runkel, R.L., Brantley, S.L., 2009.
697   Copper isotope fractionation in acid mine drainage. Geochim. Cosmochim. Acta 73, 1247–
698   1263. https://doi.org/10.1016/j.gca.2008.11.035
699 Kretzschmar, R., Schafer, T., 2005. Metal Retention and Transport on Colloidal Particles in the
700   Environment. Elements 1, 205–210. https://doi.org/10.2113/gselements.1.4.205

701 Kříbek, B., Šípková, A., Ettler, V., Mihaljevič, M., Majer, V., Knésl, I., Mapani, B., Penížek, V.,
702   Vaněk, A., Sracek, O., 2018. Variability of the copper isotopic composition in soil and
703   grass affected by mining and smelting in Tsumeb, Namibia. Chem. Geol.
704   https://doi.org/10.1016/j.chemgeo.2018.05.035
705 Lafuente, A.L., González, C., Quintana, J.R., Vázquez, A., Romero, A., 2008. Mobility of heavy
706   metals in poorly developed carbonate soils in the Mediterranean region. Geoderma 145,
707   238–244. https://doi.org/10.1016/j.geoderma.2008.03.012
708 Legros, J.P., 2007. Les grands sols du monde, Science & technologie de l'environnement. Presses
709   polytechniques et universitaires romandes.
710 Legros, S., Levard, C., Marcato-Romain, C.-E., Guiresse, M., Doelsch, E., 2017. Anaerobic
711   Digestion Alters Copper and Zinc Speciation. Environ. Sci. Technol. 51, 10326–10334.
712   https://doi.org/10.1021/acs.est.7b01662
713 Luck, J.M., Ben Othman, D., 2002a. Trace element and Pb isotope variability during rainy events
714   in the NW Mediterranean: constraints on anthropogenic and natural sources. Chem. Geol.
715   182, 443–460. https://doi.org/10.1016/S0009-2541(01)00324-2
716 Luck, J.M., Ben Othman, D., 2002b. Trace element and Pb isotope variability during rainy events
717   in the NW Mediterranean: constraints on anthropogenic and natural sources. Chem. Geol.
718   182, 443–460. https://doi.org/10.1016/S0009-2541(01)00324-2
719 Lugmair, G.., Galer, S.J.., 1992. Age and isotopic relationships among the angrites Lewis Cliff
720   86010 and Angra dos Reis. Geochim. Cosmochim. Acta 56, 1673–1694.
721   https://doi.org/10.1016/0016-7037(92)90234-A
722 Luxton, T.P., Miller, B.W., Scheckel, K.G., 2013. Zinc Speciation Studies in Soil, Sediment and
723   Environmental Samples 45.
724 Maréchal, C.N., Télouk, P., Albarède, F., 1999. Precise analysis of copper and zinc isotopic
725   compositions by plasma-source mass spectrometry. Chem. Geol. 156, 251–273.
726   https://doi.org/10.1016/S0009-2541(98)00191-0
727 Maring, H., Settle, D.M., Buat-Ménard, P., Dulac, F., Patterson, C.C., 1987. Stable lead isotope
728   tracers of air mass trajectories in the Mediterranean region. Nature 330, 154.
729 Mathur, R., Titley, S., Barra, F., Brantley, S., Wilson, M., Phillips, A., Munizaga, F., Maksaev,
730   V., Vervoort, J., Hart, G., 2009. Exploration potential of Cu isotope fractionation in
731   porphyry copper deposits. J. Geochem. Explor. 102, 1–6.
732   https://doi.org/10.1016/j.gexplo.2008.09.004
733 Mattielli, N., Petit, J.C.J., Deboudt, K., Flament, P., Perdrix, E., Taillez, A., Rimetz-Planchon, J.,
734   Weis, D., 2009. Zn isotope study of atmospheric emissions and dry depositions within a 5
735   km radius of a Pb–Zn refinery. Atmos. Environ. 43, 1265–1272.
736   https://doi.org/10.1016/j.atmosenv.2008.11.030
737 Mihaljevič, M., Jarošíková, A., Ettler, V., Vaněk, A., Penížek, V., Kříbek, B., Chrastný, V.,
738   Sracek, O., Trubač, J., Svoboda, M., Nyambe, I., 2018. Copper isotopic record in soils and
739   tree rings near a copper smelter, Copperbelt, Zambia. Sci. Total Environ. 621, 9–17.
740   https://doi.org/10.1016/j.scitotenv.2017.11.114
741 Ochoa Gonzalez, R., Weiss, D., 2015. Zinc Isotope Variability in Three Coal-Fired Power Plants:
742   A Predictive Model for Determining Isotopic Fractionation during Combustion. Environ.
743   Sci. Technol. 49, 12560–12567. https://doi.org/10.1021/acs.est.5b02402
744 Opfergelt, S., Cornélis, J.T., Houben, D., Givron, C., Burton, K.W., Mattielli, N., 2017. The
745   influence of weathering and soil organic matter on Zn isotopes in soils. Chem. Geol. 466,
746   140–148. https://doi.org/10.1016/j.chemgeo.2017.06.002

Phillips, D.L., Gregg, J.W., 2003. Source partitioning using stable isotopes: coping with too many sources. Oecologia 136, 261–269. https://doi.org/10.1007/s00442-003-1218-3

Pichat, S., Douchet, C., Albarède, F., 2003. Zinc isotope variations in deep-sea carbonates from the eastern equatorial Pacific over the last 175 ka. Earth Planet. Sci. Lett. 210, 167–178. https://doi.org/10.1016/S0012-821X(03)00106-7

Pokrovsky, O.S., Viers, J., Emnova, E.E., Kompantseva, E.I., Freydier, R., 2008. Copper isotope fractionation during its interaction with soil and aquatic microorganisms and metal oxy(hydr)oxides: Possible structural control. Geochim. Cosmochim. Acta 72, 1742–1757. https://doi.org/10.1016/j.gca.2008.01.018

Pokrovsky, O.S., Viers, J., Freydier, R., 2005. Zinc stable isotope fractionation during its adsorption on oxides and hydroxides. J. Colloid Interface Sci. 291, 192–200. https://doi.org/10.1016/j.jcis.2005.04.079

Ravel, B., Newville, M., 2005. ıt ATHENA, ıt ARTEMIS, ıt HEPHAESTUS: data analysis for X-ray absorption spectroscopy using ıt IFEFFIT. J. Synchrotron Radiat. 12, 537–541. https://doi.org/10.1107/S0909049505012719

Semlali, R.M., van Oort, F., Denaix, L., Loubet, M., 2001. Estimating Distributions of Endogenous and Exogenous Pb in Soils by Using Pb Isotopic Ratios. Environ. Sci. Technol. 35, 4180–4188. https://doi.org/10.1021/es0002621

Shiel, A.E., Weis, D., Orians, K.J., 2010. Evaluation of zinc, cadmium and lead isotope fractionation during smelting and refining. Sci. Total Environ. 408, 2357–2368. https://doi.org/10.1016/j.scitotenv.2010.02.016

Shotyk, W., Weiss, D., Heisterkamp, M., Cheburkin, A.K., Appleby, P.G., Adams, F.C., 2002. New Peat Bog Record of Atmospheric Lead Pollution in Switzerland: Pb Concentrations, Enrichment Factors, Isotopic Composition, and Organolead Species. Environ. Sci. Technol. 36, 3893–3900. https://doi.org/10.1021/es010196i

Šillerová, H., Chrastný, V., Vítková, M., Francová, A., Jehlička, J., Gutsch, M.R., Kocourková, J., Aspholm, P.E., Nilsson, L.O., Berglen, T.F., Jensen, H.K.B., Komárek, M., 2017. Stable isotope tracing of Ni and Cu pollution in North-East Norway: Potentials and drawbacks. Environ. Pollut. 228, 149–157. https://doi.org/10.1016/j.envpol.2017.05.030

Sivry, Y., Riotte, J., Sonke, J.E., Audry, S., Schäfer, J., Viers, J., Blanc, G., Freydier, R., Dupré, B., 2008. Zn isotopes as tracers of anthropogenic pollution from Zn-ore smelters The Riou Mort–Lot River system. Chem. Geol. 255, 295–304. https://doi.org/10.1016/j.chemgeo.2008.06.038

Song, S., Mathur, R., Ruiz, J., Chen, D., Allin, N., Guo, K., Kang, W., 2016. Fingerprinting two metal contaminants in streams with Cu isotopes near the Dexing Mine, China. Sci. Total Environ. 544, 677–685. https://doi.org/10.1016/j.scitotenv.2015.11.101

Sonke, J., Sivry, Y., Viers, J., Freydier, R., Dejonghe, L., Andre, L., Aggarwal, J., Fontan, F., Dupre, B., 2008. Historical variations in the isotopic composition of atmospheric zinc deposition from a zinc smelter. Chem. Geol. 252, 145–157. https://doi.org/10.1016/j.chemgeo.2008.02.006

Sossi, P.A., Halverson, G.P., Nebel, O., Eggins, S.M., 2015. Combined Separation of Cu, Fe and Zn from Rock Matrices and Improved Analytical Protocols for Stable Isotope Determination. Geostand. Geoanalytical Res. 39, 129–149. https://doi.org/10.1111/j.1751-908X.2014.00298.x

Souto-Oliveira, C.E., Babinski, M., Araújo, D.F., Andrade, M.F., 2018. Multi-isotopic fingerprints (Pb, Zn, Cu) applied for urban aerosol source apportionment and discrimination. Sci. Total Environ. 626, 1350–1366. https://doi.org/10.1016/j.scitotenv.2018.01.192

Sterckeman, T., Douay, F., Proix, N., Fourrier, H., 2000. Vertical distribution of Cd, Pb and Zn in soils near smelters in the North of France. Environ. Pollut. 107, 377–389. https://doi.org/10.1016/S0269-7491(99)00165-7

Stos-Gale, Z., Gale, N.H., Houghton, J., Speakman, R., 1995. LEAD ISOTOPE DATA FROM THE ISOTRACE LABORATORY, OXFORD: ARCHAEOMETRY DATA BASE 1, ORES FROM THE WESTERN MEDITERRANEAN. Archaeometry 37, 407–415. https://doi.org/10.1111/j.1475-4754.1995.tb00753.x

Testiati, E., Parinet, J., Massiani, C., Laffont-Schwob, I., Rabier, J., Pfeifer, H.-R., Lenoble, V., Masotti, V., Prudent, P., 2013. Trace metal and metalloid contamination levels in soils and in two native plant species of a former industrial site: Evaluation of the phytostabilization potential. J. Hazard. Mater. 248–249, 131–141. https://doi.org/10.1016/j.jhazmat.2012.12.039

Thapalia, A., Borrok, D.M., Van Metre, P.C., Musgrove, M., Landa, E.R., 2010. Zn and Cu Isotopes as Tracers of Anthropogenic Contamination in a Sediment Core from an Urban Lake. Environ. Sci. Technol. 44, 1544–1550. https://doi.org/10.1021/es902933y

Véron, A., Flament, P., Bertho, M.L., Alleman, L., Flegal, R., Hamelin, B., 1999. Isotopic evidence of pollutant lead sources in Northwestern France. Atmos. Environ. 33, 3377–3388. https://doi.org/10.1016/S1352-2310(98)00376-8

Viers, J., Grande, J.A., Zouiten, C., Freydier, R., Masbou, J., Valente, T., Torre, M.-L. de la, Destrigneville, C., Pokrovsky, O.S., 2018. Are Cu isotopes a useful tool to trace metal sources and processes in acid mine drainage (AMD) context? Chemosphere 193, 1071–1079. https://doi.org/10.1016/j.chemosphere.2017.11.133

Viers, J., Oliva, P., Nonell, A., Gélabert, A., Sonke, J.E., Freydier, R., Gainville, R., Dupré, B., 2007. Evidence of Zn isotopic fractionation in a soil–plant system of a pristine tropical watershed (Nsimi, Cameroon). Chem. Geol. 239, 124–137. https://doi.org/10.1016/j.chemgeo.2007.01.005

Voegelin, A., Jacquat, O., Pfister, S., Barmettler, K., Scheinost, A.C., Kretzschmar, R., 2011. Time-Dependent Changes of Zinc Speciation in Four Soils Contaminated with Zincite or Sphalerite. Environ. Sci. Technol. 45, 255–261. https://doi.org/10.1021/es101189d

Voegelin, A., Pfister, S., Scheinost, A.C., Marcus, M.A., Kretzschmar, R., 2005. Changes in zinc speciation in field soil after contamination with zinc oxide. Env. Sci Technol 39, 6616.

von Storch, H., Costa-Cabral, M., Hagner, C., Feser, F., Pacyna, J., Pacyna, E., Kolb, S., 2003. Four decades of gasoline lead emissions and control policies in Europe: a retrospective assessment. Sci. Total Environ. 311, 151–176. https://doi.org/10.1016/S0048-9697(03)00051-2

Weinstein, C., Moynier, F., Wang, K., Paniello, R., Foriel, J., Catalano, J., Pichat, S., 2011. Isotopic fractionation of Cu in plants. Chem. Geol. https://doi.org/10.1016/j.chemgeo.2011.05.010

Weiss, D., Shotyk, W., Boyle, E.A., Kramers, J.D., Appleby, P.G., Cheburkin, A.K., 2002. Comparative study of the temporal evolution of atmospheric lead deposition in Scotland and eastern Canada using blanket peat bogs. Sci. Total Environ. 292, 7–18. https://doi.org/10.1016/S0048-9697(02)00025-6

836 Weiss, D.J., Rehkdmper, M., Schoenberg, R., McLaughlin, M., Kirby, J., Campbell, P.G.C.,
837   Arnold, T., Chapman, J., Peel, K., Gioia, and S., 2008. Application of Nontraditional
838   Stable-Isotope Systems to the Study of Sources and Fate of Metals in the Environment.
839   Environ. Sci. Technol. 42, 655–664. https://doi.org/10.1021/es0870855
840 Wen, H., Zhang, Y., Cloquet, C., Zhu, C., Fan, H., Luo, C., 2015. Tracing sources of pollution in
841   soils from the Jinding Pb–Zn mining district in China using cadmium and lead isotopes.
842   Appl. Geochem. 52, 147–154. https://doi.org/10.1016/j.apgeochem.2014.11.025
843 Wiederhold, J.G., 2015. Metal Stable Isotope Signatures as Tracers in Environmental
844   Geochemistry. Environ. Sci. Technol. 49, 2606–2624. https://doi.org/10.1021/es504683e
845 Wilkinson, J.J., Weiss, D.J., Mason, T.F.D., Coles, B.J., 2005. Zinc isotope variation in
846   hydrothermal systems: preliminary evidence from the Irish Midlands ore field 8.
847 World Health Organization, Food and Agriculture Organization of the United Nations,
848   International Atomic Energy Agency (Eds.), 1996. Trace elements in human nutrition and
849   health. World Health Organization, Geneva.
850 Yanful, E.K., Quigley, R.M., Wayne Nesbitt, H., 1988. Heavy metal migration at a landfill site,
851   Sarnia, Ontario, Canada—2: metal partitioning and geotechnical implications. Appl.
852   Geochem. 3, 623–629. https://doi.org/10.1016/0883-2927(88)90094-7
853 Yin, N.-H., Sivry, Y., Benedetti, M.F., Lens, P.N.L., van Hullebusch, E.D., 2016. Application of
854   Zn isotopes in environmental impact assessment of Zn–Pb metallurgical industries: A mini
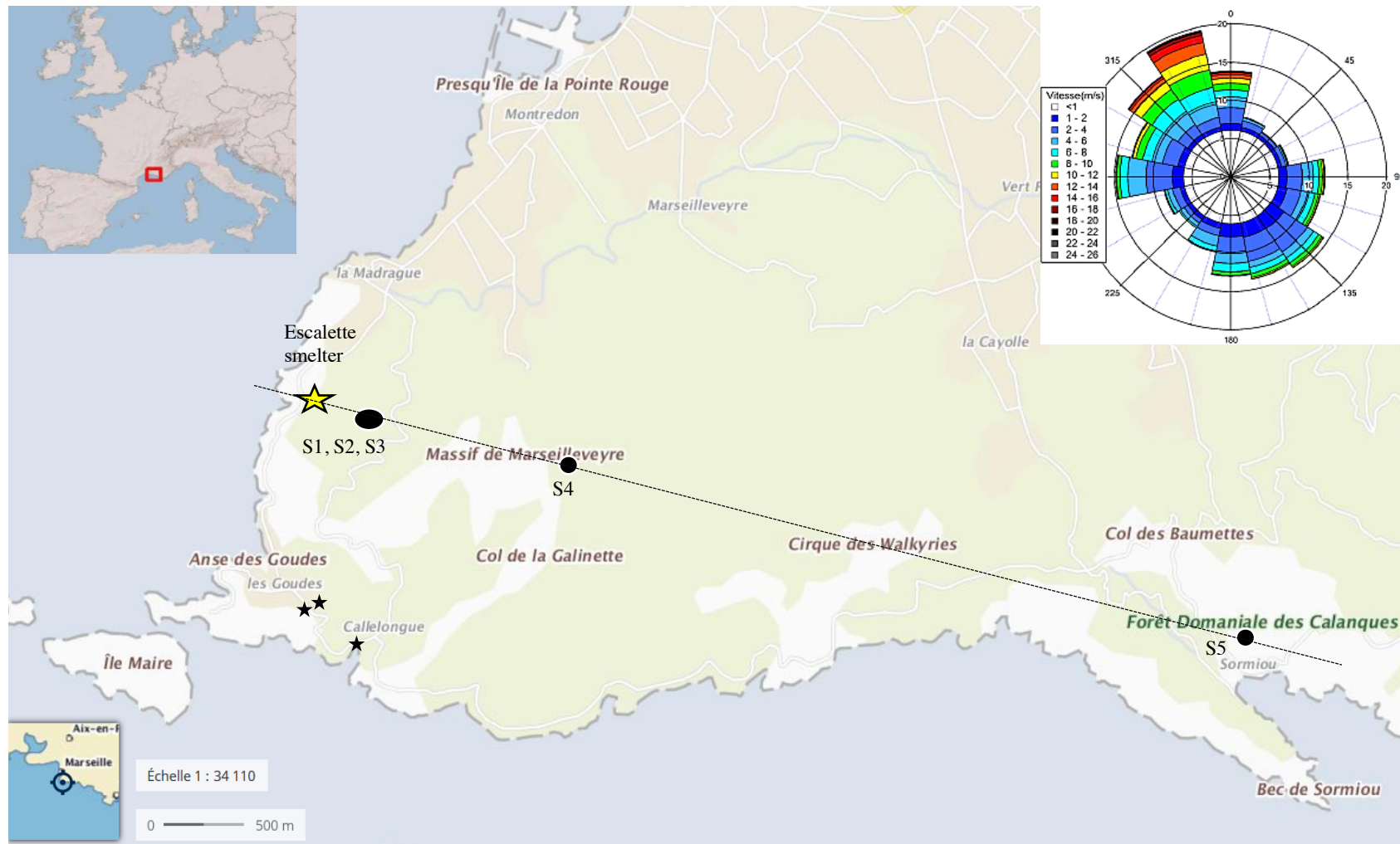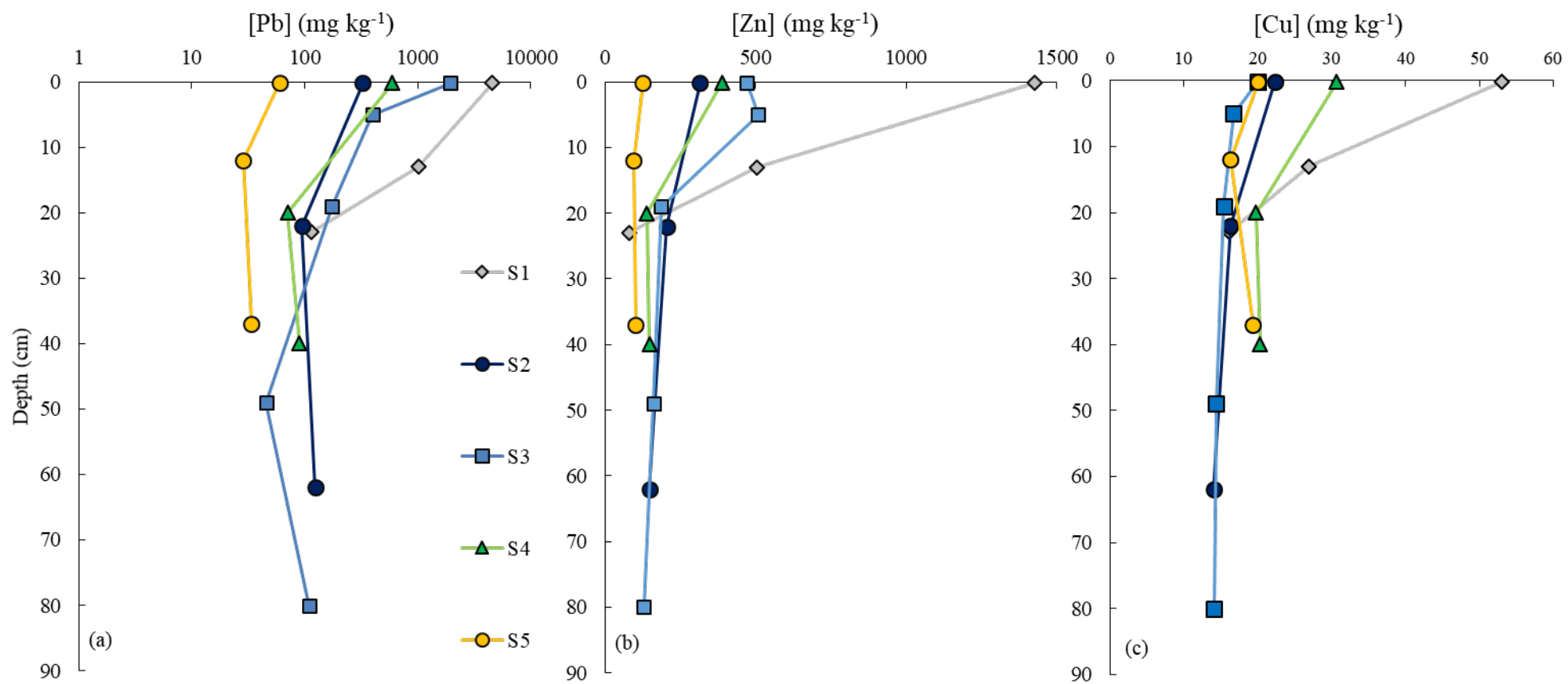855   review. Appl. Geochem. 64, 128–135. https://doi.org/10.1016/j.apgeochem.2015.09.016
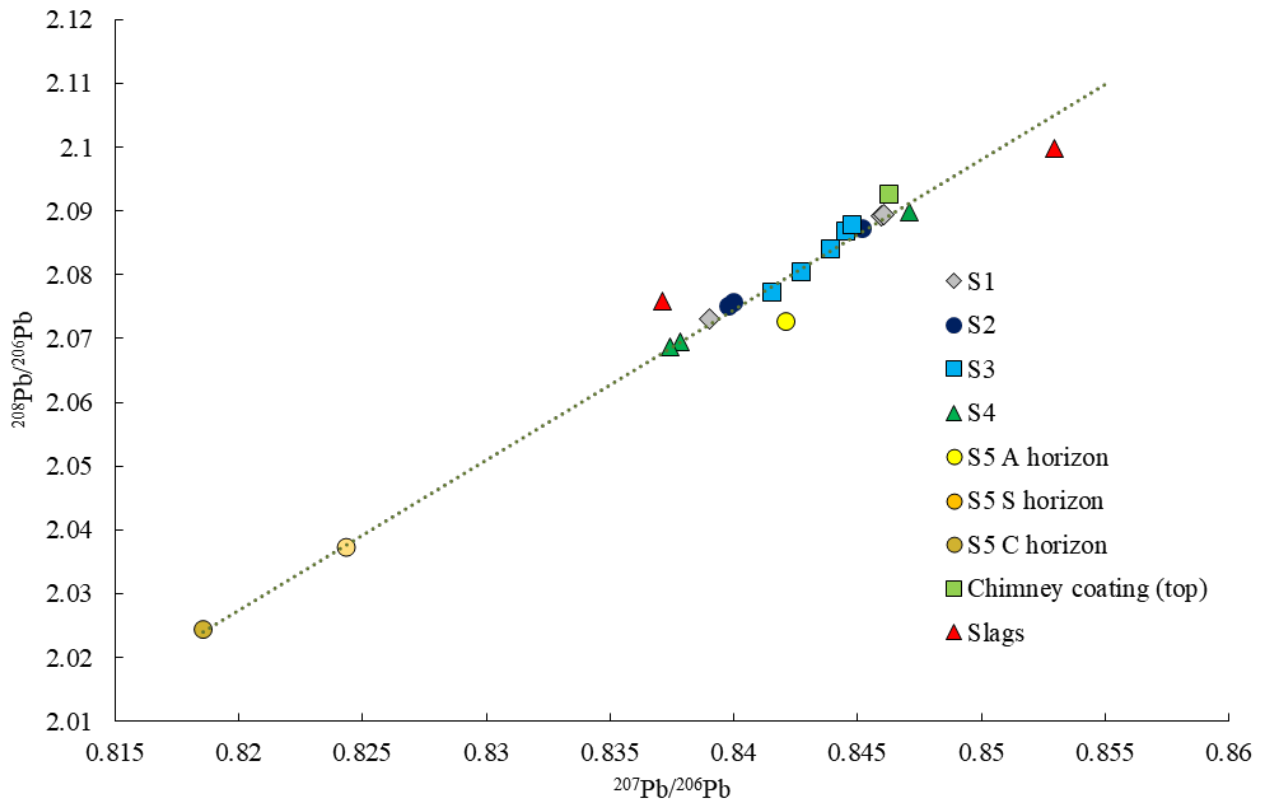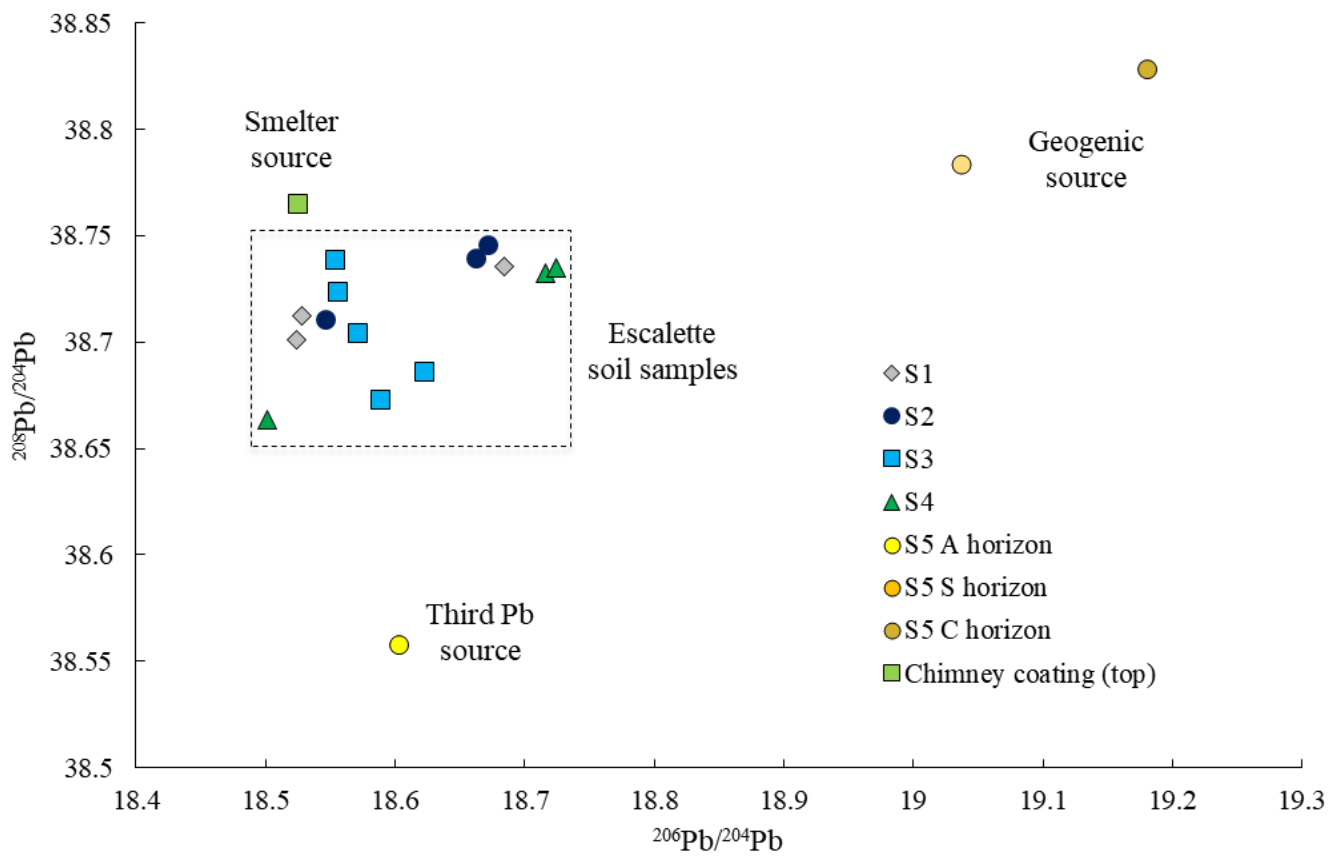856

Figure 1

Figure 2

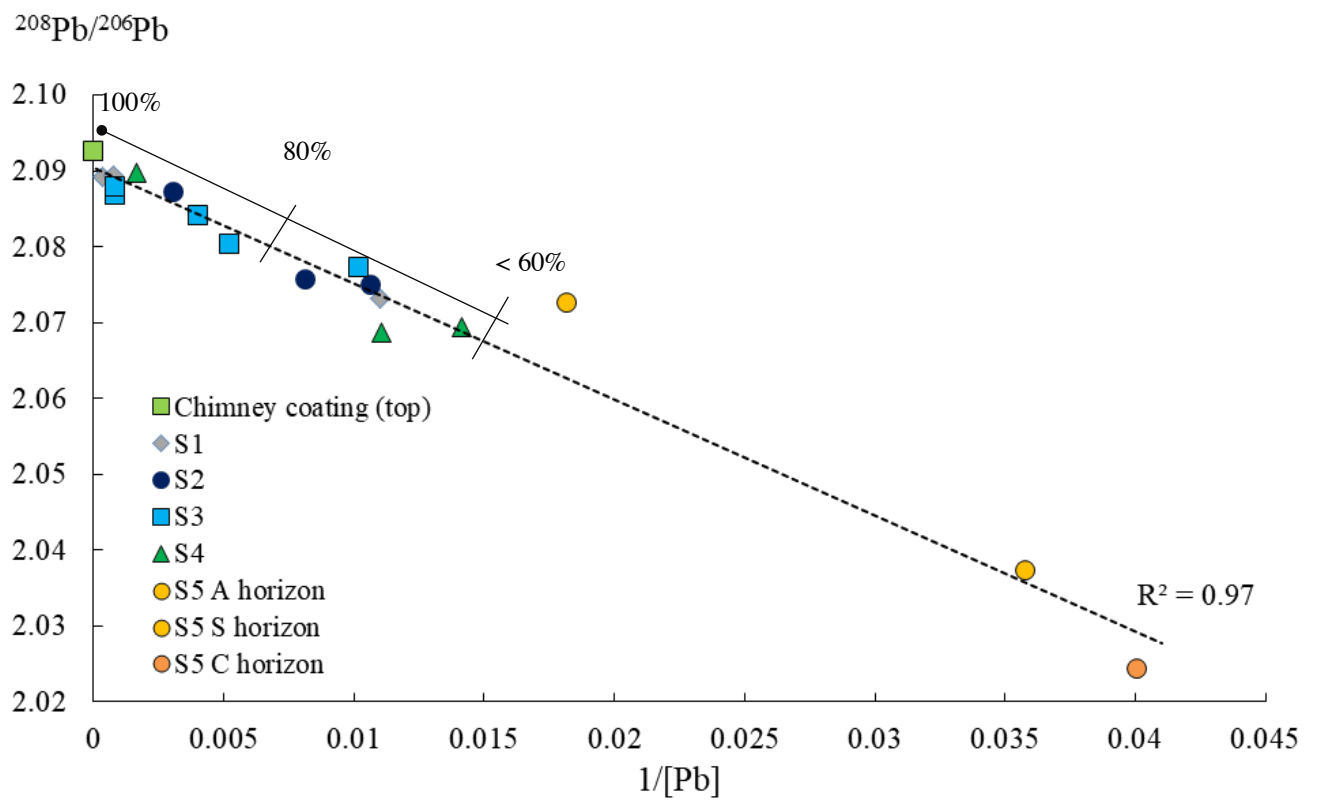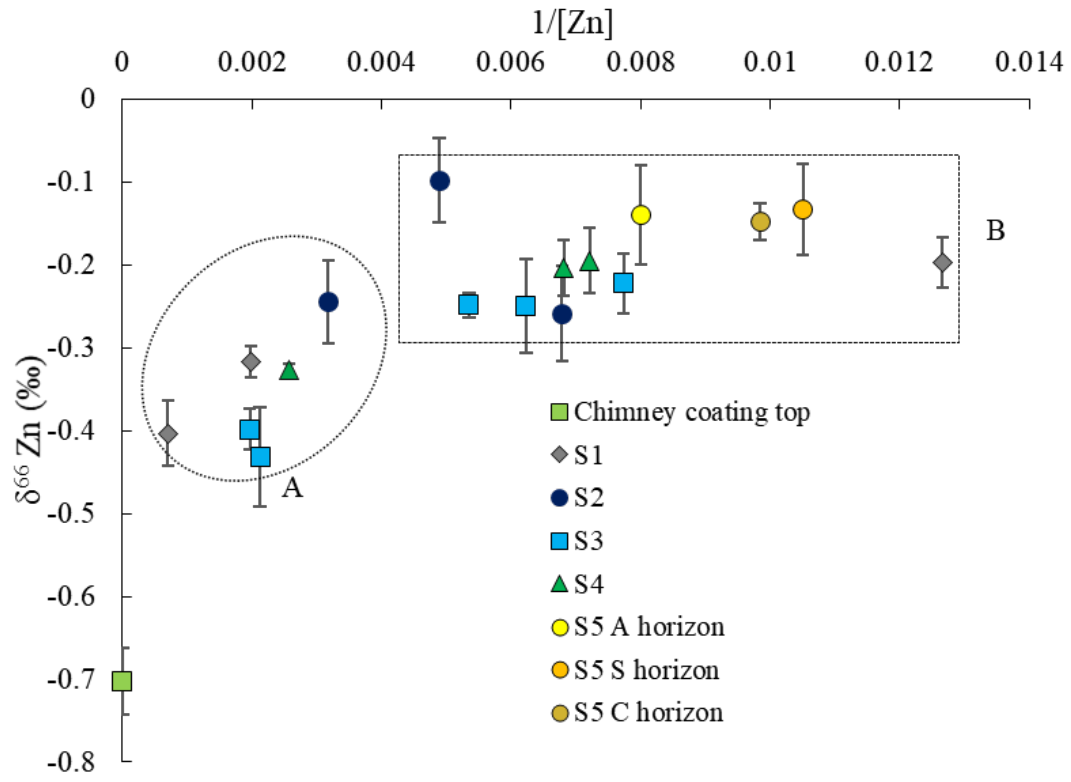Figure 3

Figure 4a

Figure 4b

Figure 5

Figure 6

Figure Captions

Figure 1: Global Marseilleveyre Massif map near Marseilles (France). Average wind directions over 10 years (2001-2011) obtained from Marignane station (MétéoFrance, 2011). Dotted line indicates the 7 km NW-SE studied transect with relative position of the soil profiles under the main wind NNW from the Escalette smelter (yellow star) to S5 soil (black dot). Black stars highlight the position of other industries (Pb smelter (1854-1878), soda-production factory (1854-1894), sulfur refinery (1860-1900) operating at the beginning of the Escalette smelter exploitation (1851-1925).

Figure 2: Concentration (mg kg^{-1}) profiles of Pb (a), Zn (b) and Cu (c) in sampled soils. For Pb concentrations (a) note the logarithmic scale.

Figure 3: Evolution of Pb (a), Zn (b) and Cu (c) isotopic signatures of soils with depth. For clarity, results obtained on the smelter samples (slags and chimney) are placed above the surface level. Error bars represent the two standard deviations (2SD) calculated from three analyses of the same sample. Calculated 2SD for Pb ratios are $<10^{-4}$ and are printed in smaller type than the symbols. In the ^{208}Pb/^{206}Pb plot (a), the two chimney coatings (top and bottom) overlap due to their identical Pb isotopic compositions. Soil sample symbols are placed at the top of their respective horizons. Only two slags (1,2) were analyzed for their Pb isotopic signatures while 7 slags were analyzed for Zn and Cu.

Figure 4a: Mixing trend of all sampled soils and smelter samples in a ^{208}Pb/^{206}Pb vs ^{207}Pb/^{206}Pb plot. Calculated 2SD for Pb ratios are $<10^{-4}$ and are printed in smaller type than the symbols. End members are represented by (i) the uncontaminated deepest horizon of the S5 profile (S5 C) and (ii) the chimney coatings. The dotted line represents the linear trend ($r^2 = 0.98$, p value=1.47E^{-16}). For a given soil profile (except for S5), all horizons are represented by identical symbols. For S5, individual horizons are distinguished using the same symbols but different

colors. Only slags 1 and 2 were analyzed for Pb isotopic compositions and are presented here (see Table S1c).

Figure 4b: Plot of $^{208}Pb/^{204}Pb$ vs $^{206}Pb/^{204}Pb$. Lead isotopes of the Escalette soil samples (highlighted by the dotted black square) are constrained in a three Pb source domain: smelter source (i.e. the chimney coating top), geogenic source (i.e. S5 deepest horizon) and a third source (i.e. atmospheric aerosol) only visible on the S5 A horizon. Calculated 2SD for Pb ratios are $<10^{-4}$ and printed smaller than the symbols.

Figure 5: Plot of $^{208}Pb/^{206}Pb$ vs 1/[Pb] total concentrations. A two end-member mixing line (dotted line, $r^2=0.97$; p value=$2.84E^{-13}$) connects the chimney sample (top) and the deepest horizon of the S5 profile (C). Soils from S1 to S4 plotted along the mixing line, indicating that their total Pb concentrations represent a mixture of anthropogenic Pb from the smelter ($^{208}Pb/^{206}Pb$: 2.0922), and natural Pb, from the geogenic background ($^{208}Pb/^{206}Pb$: 2.0243). The contribution of anthropogenic Pb to the total Pb (%), presented in Table S, is reported as a solid black line, close to the mixing line.

Figure 6: Plot of $\delta^{66}Zn$ values (‰) vs 1/[Zn]. Zinc isotopic signatures of the soils cannot be explained by binary mixing. Two distinct Zn pools, labeled A and B, and highlighted by a circle and rectangle in dashed lines can be distinguished. Error bars represent the 2SD associated to $\delta^{66}Zn$ values. A: pool dominated by anthropogenic Zn from the smelter, observed in S1, S2, S3 and S4 surface horizons. Discrepancy between $\delta^{66}Zn$ values of the soils and the chimney sample can be explained by isotopic fractionation during precipitation of Zn-Layered-Double-Hydroxide in the surface horizons. B: pool dominated by natural Zn observed in all other subsurface horizons and in the S5 soil profile and originating from the natural geogenic background modified by pedogenetic processes.